Siriusly, a newly identified intermediate-age Milky Way stellar cluster: a spectroscopic study of Gaia 1

Siriusly, a newly identified intermediate-age Milky Way stellar cluster: a spectroscopic study of Gaia 1

J. D. Simpson,[1,2,3]⋆ G. M. De Silva,[1,4] S. L. Martell,[5] D. B. Zucker,[1,2,3]
A. M. N. Ferguson,[6] E. J. Bernard,[7] M. Irwin,[8] J. Penarrubia[6] and E. Tolstoy[9]

[1]*Australian Astronomical Observatory, 105 Delhi Rd, North Ryde, NSW 2113, Australia*
[2]*Department of Physics and Astronomy, Macquarie University, Sydney NSW 2109, Australia*
[3]*Research Centre in Astronomy, Astrophysics and Astrophotonics, Macquarie University, Sydney NSW 2109, Australia*
[4]*Sydney Institute for Astronomy, School of Physics, A28, The University of Sydney, Sydney NSW 2006, Australia*
[5]*School of Physics, University of New South Wales, Sydney NSW 2052, Australia*
[6]*Institute for Astronomy, University of Edinburgh, Blackford Hill, Edinburgh EH9 3HJ, UK*
[7]*Université Côte d'Azur, OCA, CNRS, Lagrange, France*
[8]*Institute of Astronomy, University of Cambridge, Madingley Road, Cambridge, CB3 0HA, UK*
[9]*Kapteyn Astronomical Institute, University of Groningen, Landleven 12, 9747AD Groningen, Netherlands*

ABSTRACT

We confirm the reality of the recently discovered Milky Way stellar cluster Gaia 1 using spectra acquired with the HERMES and AAOmega spectrographs of the Anglo-Australian Telescope. This cluster had been previously undiscovered due to its close angular proximity to Sirius, the brightest star in the sky at visual wavelengths. Our observations identified 41 cluster members, and yielded an overall metallicity of [Fe/H] $= -0.13 \pm 0.13$ and barycentric radial velocity of $v_\mathrm{r} = 58.30 \pm 0.22 \,\mathrm{km\,s^{-1}}$. These kinematics provide a dynamical mass estimate of $12.9^{+4.6}_{-3.9} \times 10^3 \,\mathrm{M_\odot}$. Isochrone fits to *Gaia*, 2MASS, and Pan-STARRS1 photometry indicate that Gaia 1 is an intermediate age ($\sim$3 Gyr) stellar cluster. Combining the spatial and kinematic data we calculate Gaia 1 has a circular orbit with a radius of about 12 kpc, but with a large out of plane motion: $z_\mathrm{max} = 1.1^{+0.4}_{-0.3}$ kpc. Clusters with such orbits are unlikely to survive long due to the number of plane passages they would experience.

Key words: catalogues – Galaxy: general – Galaxy: structure.

1 INTRODUCTION

The ESA *Gaia* mission has the goal of constructing the largest and most precise 6D space catalogue ever made. It is measuring the positions, distances, space motions and many physical characteristics of some 1 billion stars in our Galaxy and beyond (Prusti et al. 2016). The first data release (Brown et al. 2016) has already been used to identify previously unknown comoving pairs of stars (Andrews, Chanamé & Agüeros 2017; Oh et al. 2017), determine parallactic distances to globular clusters (Watkins & van der Marel 2017), measure the proper motion of the distant globular cluster NGC 2419 by combining *Gaia* and *HST* data (Massari et al. 2017), and show that M40 is in fact just two unrelated stars and not a true binary (Merrifield, Gray & Haran 2016).

Koposov, Belokurov & Torrealba (2017) took advantage of a number of unique capabilities of *Gaia* (i.e. no weather and sky brightness variations; low-to-no spurious detections; excellent

star/galaxy discrimination) to search for stellar overdensities using a modified method they had previously applied with great success to ground-based surveys (e.g. Koposov et al. 2007, 2015). Their search of the *Gaia* catalogue identified 259 candidates overdensities, of which 244 had clear associations with previously known clusters and dwarf galaxies. Of the unknown overdensities, two were statistically significant enough to warrant quick publication: Gaia 1 and *Gaia* 2. Of particular note is Gaia 1 which is located only 11 arcmin from Sirius (though their physical separation is ∼4 kpc), the brightest star in the night sky. This cluster likely would have been previously identified had it not been for this proximity, which has hidden its existence from astronomers.

Beyond the novelty of being previously undiscovered, the cluster parameters estimated by Koposov et al. (2017) – 6 Gyr, 14 000 M$_\odot$, [Fe/H] $= -0.7$ – suggest that Gaia 1 is an interesting target in its own right due to its being on the border between open and globular clusters. It is about 1 kpc out of the plane of the Galaxy, which might suggest it is an open cluster. The photometry shows a populated red clump region, indicative of an intermediate age,

⋆ E-mail: jeffrey.simpson@aao.gov.au

metal-rich cluster (see the review by Girardi 2016, and references therein). However, the available photometry can only provide so much information, with a complete picture of the cluster's chemistry and kinematic only possible when the photometry is combined with spectroscopy.

It is important to spectroscopically observe purported clusters to confirm that the stars truly have similar kinematics and chemistry. As an example, Lodén 1 (Loden 1980) had been catalogued as a 2-Gyr stellar cluster at a heliocentric distance of 360 pc in the Database for Galactic Open Clusters (WEBDA, Mermilliod & Paunzen 2003). Such properties would make it a very useful old, nearby cluster target for calibration and benchmarking of large stellar surveys. But when Han, Curtis & Wright (2016) investigated the photometry and kinematics of the cluster, they determined that Lodén 1 was 'neither old, nor nearby, nor a cluster!'. The positional and kinematic information of *Gaia*, combined with the chemical information of large stellar surveys (e.g. GALAH, APOGEE, Gaia-ESO, 4MOST, WEAVE) will likely lead to the 'de-identification' of several other putative clusters.

In this paper, we confirm that Gaia 1 is a kinematically distinct cluster of stars, using spectra acquired with the Anglo-Australian Telescope HERMES and AAOmega spectrographs. This paper is structured as follows: Section 2 details the observations; Section 3 explains how the radial velocities were determined for the stars; Section 4 discusses the metallicities estimated from the high-resolution HERMES spectra and estimated from the CaT lines in the AAOmega spectra; Section 5 combines the radial velocity and metallicity information to identify members; and Section 6 discusses the results and what they mean for the overall cluster properties and its orbit.

2 OBSERVATIONS

Gaia 1 was observed with two of the spectrographs of the 3.9-m *Anglo-Australian Telescope* over three nights: on the night of 2017 February 15 with the four-armed high-resolution HERMES spectrograph, and on the nights of 2017 February 24 and 26 with the two-armed AAOmega spectrograph. For all the observations, the light was fed to the instruments using the 392-fibre two-degree field (2dF) optical fibre positioner top-end (Lewis et al. 2002).

HERMES simultaneously acquires spectra using four independent cameras with non-contiguous wavelength coverage totalling $\sim$1000 Å at a spectral resolution of $R \approx 28\,000$ (Sheinis et al. 2015). Its fixed wavelength bands were chosen primarily for the on-going GALAH survey (blue: 4715–4900 Å; green: 5649–5873 Å; red: 6478–6737 Å; near-infrared: 7585–7887 Å; De Silva et al. 2015; Martell et al. 2017).

AAOmega simultaneously acquires spectra using independent blue and red cameras (Sharp et al. 2006). For these observations, the blue camera was fitted with the 580 V grating ($R \sim 1200$; 3700–5800 Å) and the red camera fitted with the 1700 D grating ($R \sim 10\,000$; 8340–8840Å). The latter grating is designed for observations of the near-infrared calcium triplet lines around 8600Å, which allows for metallicity estimation and precise radial velocity measurement.

Gaia 1 is located at RA = $6^{\mathrm{h}}45^{\mathrm{m}}53^{\mathrm{s}}$, Dec = $-16^{\circ}45'00''$ and has an angular extent of $\sim$15 arcmin. As mentioned in Section 1, the centre of Gaia 1 is located only 11 arcmin from the $V = -1.5$ Sirius system. This meant we had two main concerns when observing Gaia 1: that diffraction spikes from Sirius could coincide with fibres and that the scattered light from Sirius could be so

large as to overwhelm the light from the target stars which are 13–18 mag fainter. The extent and brightness of the diffraction spikes from Sirius were difficult to predict, so our primary mitigation method was to simply avoid placing fibres within 10 arcmin of Sirius. To reduce the scattered light from Sirius we used the 2dF plate that was coated black, and the field was centred on Sirius, with the cluster off-centre. Placing the cluster off-centre does have the trade-off of reducing the number of targets that can be observed, as the fibres of 2dF have a maximum allowed offset from their radial positions, and cannot be placed across the centre of the plate.

The observed targets were selected from a catalogue created by cross-matching *Gaia* DR1 with The Two Micron All Sky Survey (2MASS) catalogue (Skrutskie et al. 2006). This cross-match was performed using the *Gaia* archive and joining their `gaia_source`, `tmass_best_neighour` and `tmass_original_valid` tables on `source_id` and `tmass_oid`. For the target identification within the Panoramic Survey Telescope and Rapid Response System Data Release 1 (Pan-STARRS1 or PS1; Chambers et al. 2016; Magnier et al. 2016), a closest neighbour positional search was used between the *Gaia*-2MASS table and a table created from PS1's `ObjectThin` and `MeanObject` tables, with a minimum of 11 PS1 epoch detections. We found that 11 detections of an object were the minimum required to remove the large number of spurious objects in PS1 associated with the diffraction pattern of Sirius in the PS1 images. For the 1 deg around Sirius, there were a median of 56 detections per target in our final catalogue.

For the HERMES observations, the highest priority targets were those within 5 arcmin of the cluster centre that photometry showed were in the prominent red clump (or red horizontal branch; 15 candidates observed), with the next highest priority given to the likely red giant branch (RGB) members (eight candidates). Lower priority targets were those in an annulus from 5–10 arcmin from the cluster and still photometrically located in either the clump or on the RGB (17 candidates). A further 287 stars were observed across the full 2 deg field within the magnitude range of $12 < G < 14$ and no colour cuts. The locations of the observed targets are shown on the colour–magnitude diagrams (CMD) in Fig. 1. We also allocated 50 fibres to sky positions as it was unclear how bright the sky background would be due to the proximity of Sirius. The field was observed for three 20-min exposures along with the standard exposures of the fibre flat lamps and the ThXe arc lamp.

On the AAOmega nights, we concentrated on fainter stars within 7 arcmin of the cluster centre, with a selection of potential sub-giant branch (SGB) stars ($1.5 < G - K_{\mathrm{S}} < 3.3$; $17.4 > G > 16.5$; 42 candidates observed) and lower RGB stars ($1.5 < G - K_{\mathrm{S}} < 2.3$; $16.5 > G > 15.1$; 56 candidates). On the first night, 12 of the clump stars that had been identified as members from the HERMES spectra were also re-observed. We observed an additional 571 stars randomly chosen across the full 2 deg field of view that were in the magnitude and colour cuts of the AAOmega RGB and SGB selections. These targets were divided into two fields, with one field observed on each night. The locations of the observed targets are shown on the CMD in Fig. 1. The standard 25 sky fibres were used on both AAOmega nights, as the results from the HERMES observations confirmed that removing the sky background from Sirius was not going to be a problem. On the first night, we obtained three 20-min exposures and on the second night four 20-min exposures, along with the standard exposures of the fibre flat lamp and arc lamps. Unfortunately, it was found that the blue AAOmega spectra were dominated by scattered light from Sirius and therefore could not be analysed for this work.
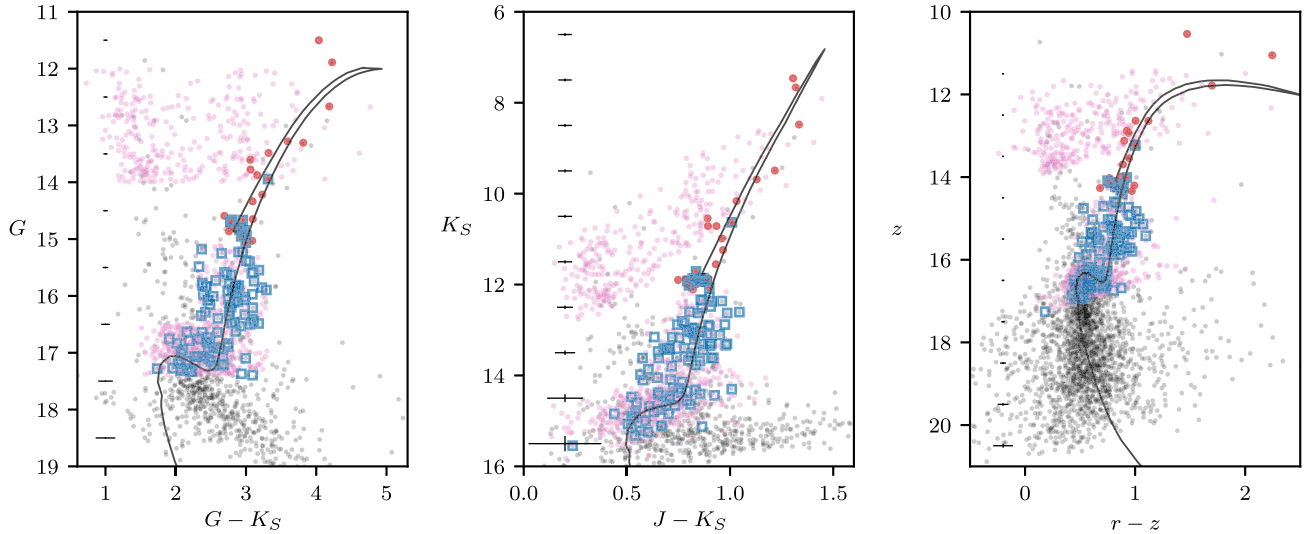
Figure 1. CMD of Gaia 1 in the various photometric catalogues. The left-hand panel is *Gaia G* and 2MASS K_S, middle panel is 2MASS J and K_S and the right-hand panel is PS1 *r* and *z*. The PARSEC (version 1.2S) isochrone is for a metallicity [M/H] = −0.2 and age of 3.5 Gyr. The black dots are all stars found in each of the *Gaia*, 2MASS and Pan-STARRS1 catalogues within 7 arcmin of the cluster centre. Overplotted are the stars observed by HERMES (red dots) and AAOmega (blue squares) within 10 arcmin of the cluster. Errorbars show the 2σ error in magnitude and colour in 1 mag bins. These were the stars considered most likely to be members. The pink dots show the remaining stars that were observed across the entire 2dF field of view. For the HERMES observations these had no colour cuts, while for the AAOmega observations, these potential extratidal stars were restricted to the same colour and magnitude regions as the sub-giant branch and lower red giant branch observations.

For both the HERMES and AAOmega observations, the raw spectra were reduced using the AAO's 2DFDR reduction software (AAO Software Team 2015, version 6.28) with the defaults for the particular spectrograph and gratings. Examples of the final reduced spectra for five red clump stars are shown in Fig. 2.

3 RADIAL VELOCITIES

For the stars observed with HERMES, the barycentric radial velocity was measured independently from the spectra of the blue, green and red cameras[1] by cross-correlating the observed spectra with a template of the cool giant Arcturus. This was implemented with ISPEC, an open source framework for spectral analysis (Blanco-Cuaresma et al. 2014). The average value obtained from the three cameras was adopted as the radial velocity of the star. 24 of the 327 stars observed returned inconsistent radial velocities between the three arms ($\sigma_V > 10\,\mathrm{km\,s^{-1}}$). Inspection of their spectra and location on the CMD revealed that they all tended to be the bluest stars observed ($G - K_S < 1.5$) and therefore are likely hot dwarfs that are too dissimilar from Arcturus for cross-correlation to work successfully.

For the red AAOmega spectra, the near-infrared calcium triplet (CaT) lines at 8498.03, 8542.09 and 8662.14 Å (Edlén & Risberg 1956) were used to measure the barycentric radial velocities of the stars and to estimate their metallicity (for discussion of the metallicity results from the CaT lines, see Section 4.2). We direct the readers to Simpson et al. (2017) for a full description of the method used to measure the radial velocities and equivalent widths of the CaT lines. Briefly, the spectra were normalized with a fifth-degree Chebyshev polynomial using SCIPY's CHEBFIT function and each CaT line fitted with a Voigt function provided by

---

[1] The near-infrared spectrum acquired by HERMES is partially dominated by terrestrial atmospheric bands, which make radial velocity measurements via cross-correlation difficult.
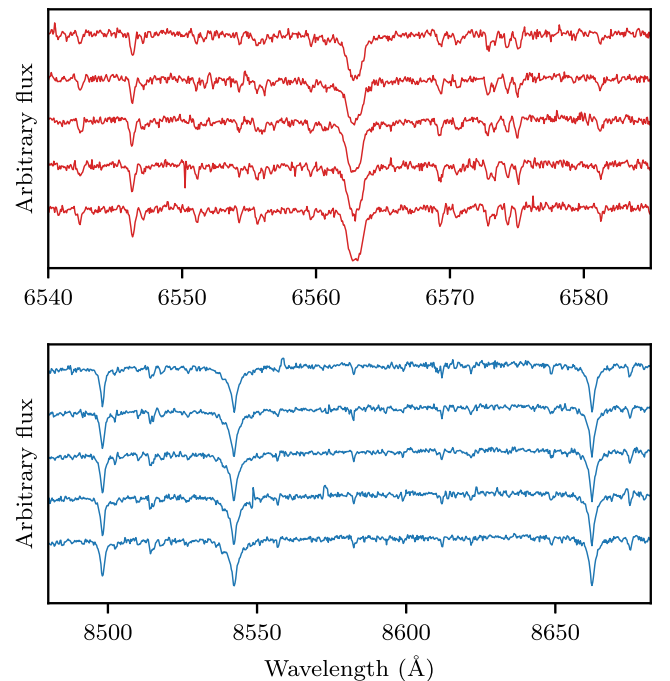

Figure 2. Examples of the reduced spectra for five clump stars. Top: a portion of the HERMES spectra centred on the Hα line. Bottom: the same stars, showing their red AAOmega spectra and the calcium triplet lines. $\mathrm{SNR_{HERMES}} \approx 30$ per pixel and $\mathrm{SNR_{AAOmega}} \approx 50$, with the stars having G magnitudes of about 14.8 (i.e. the faintest HERMES stars and the brightest AAOmega stars).

the VOIGT1D (McLean, Mitchell & Swanston 1994) function from ASTROPY (Robitaille et al. 2013). The central wavelength of the fitted Voigt functions was found and the average of the three line values adopted as the radial velocity of the star. This was repeated for 100 realizations with random Gaussian noise added to each wavelength

pixel to understand the uncertainties of the method. The equivalent widths of the lines used for metallicity estimation (see Section 4.2) were found from the fitted Voigt functions.

There were 12 stars observed with both HERMES and AAOmega. The top panel of Fig. 3 shows a comparison of the velocities derived from the two sets of observations; the consistency is on the $\lesssim 1\,\mathrm{km\,s^{-1}}$ level. Inspection of the radial velocities of the candidates showed the strong velocity signature of the cluster. Of the 40 candidates observed by HERMES within 10 arcmin of the cluster, 29 stars had radial velocities with $56 < r_v < 61\,\mathrm{km\,s^{-1}}$ (Fig. 3c). For those stars observed with AAOmega, in addition to the 12 stars in common with the HERMES observations, there were 21 probable members identified from their radial velocities using the velocity cut defined from the HERMES observations. Combining the results from the two data sets we find that the systemic radial velocity and dispersion of the cluster is $v_r = 58.30 \pm 0.22\,\mathrm{km\,s^{-1}}$ with a dispersion of $\sigma_v = 0.94 \pm 0.15\,\mathrm{km\,s^{-1}}$ (for just the HERMES sample $v_r = 58.30 \pm 0.10\,\mathrm{km\,s^{-1}}$ and $\sigma_v = 0.86 \pm 0.09\,\mathrm{km\,s^{-1}}$; and for just the AAOmega sample $v_r = 58.20 \pm 0.01\,\mathrm{km\,s^{-1}}$ and $\sigma_v = 1.0 \pm 0.01\,\mathrm{km\,s^{-1}}$).

4 METALLICITIES

The metallicities of the probable cluster members identified in Section 3 were inferred from both the HERMES (Section 4.1) and AAOmega spectra (Section 4.2).

4.1 HERMES spectra

For the stars observed with HERMES and identified as members in Section 3, stellar parameters were determined from the high-resolution spectra with the classical method. The equivalent widths of the neutral iron lines were measured using ARES2 (Sousa et al. 2015) and the ionized iron lines using IRAF, and then the 1D LTE abundance for each line was calculated with MOOG (Sneden 1973) using Kurucz model atmospheres interpolated from the Castelli & Kurucz (2004) grid of model atmospheres. The spectroscopic T_{eff} was derived by requiring excitation equilibrium of Fe I lines. The log g was derived via ionization equilibrium, i.e. requiring the abundances from Fe I lines to equal those from Fe II lines. For comparison, we also computed photometric gravities via the Stefan–Boltzmann relation, using our spectroscopically derived T_{eff}, bolometric corrections calculated from table 12 of Jordi et al. (2010), a distance modulus of $(m - M)_G = 14.50$, and with a stellar mass of $1.5\,\mathrm{M_\odot}$. Microturbulence was derived from the condition that abundances from Fe I lines show no trend with equivalent width. For the 27 stars with reliable metallicity values, we find an average metallicity (and standard deviation of the sample) of $[\mathrm{Fe/H}] = -0.13 \pm 0.13$. The results for each star are found in Table B1. Uncertainties for the metallicities were found from the standard deviation of the Fe abundances found for each individual iron line divided by the square root of the number of iron lines used for each star.

While this paper was in preprint, Mucciarelli et al. (2017) presented an analysis of six He-clump stars in Gaia 1 based on spectra taken with the Magellan MIKE spectrograph. They note that the surface gravities we derive spectroscopically for some of our stars are 0.5 dex, too high relative to an isochrone with age of 3 Gyr and solar metallicity (similar to our favoured values of 3.5 Gyr and $[\mathrm{Fe/H}] = -0.2$). Our HERMES spectra are lower signal than one would typically use for accurate spectroscopic abundance determination (due to limitations of telescope time available). However, as none of our primary conclusions depend on spectroscopic gravities,
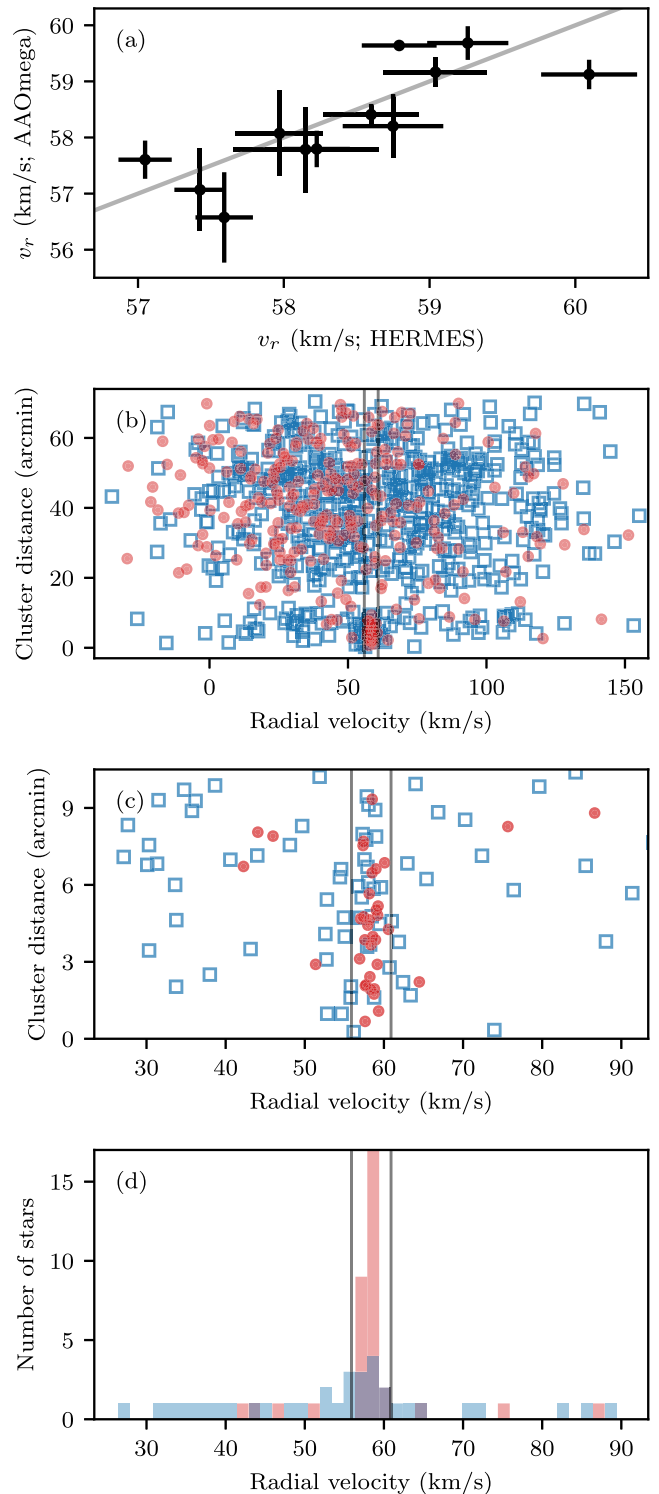

Figure 3. Radial velocity results. (a) Comparison of the radial velocity derived from the HERMES and AAOmega spectra for the stars in common. The line is the one-to-one line. (b) The radial velocities of all of the stars against their distance from the cluster centre of Gaia 1. Stars observed with HERMES are red dots and stars observed with AAOmega are blue squares. The lower density of targets observed in the range of 10–20 arcmin is due to the Sirius exclusion zone. (c) The same as (b) but showing only the inner 10 arcmin. (d) Histogram of the inner 10 arcmin, again with the HERMES velocity used for doubly observed stars. The vertical lines in (b)–(d) indicate the velocities used to define the radial velocity range of probable cluster members.

Table 1. Distance moduli and reddening determined by isochrone fitting (see Section 6) from *Gaia*, 2MASS, PS1 photometry. $(m - M)_0$ was determined for each using extinctions for different bandpasses determined by Schlafly & Finkbeiner (2011). They have not determined the values for *Gaia G* so no transformation was done.

		$(m - M)_X$	$E(A - B)$	$(m - M)_0$	d (kpc)
G	$G - K_S$	14.50	0.80		
K_S	$J - K_S$	13.45	0.27	13.2	4.5
r	$r - z$	13.74	0.53	13.1	4.1

we do not believe this limitation will have had any impact on the nature, mass, age, stellar membership or orbit we find for Gaia 1, or the metallicities we derive from the CaT region of the AAOmega spectra. Indeed, within the uncertainties, our measurements of [Fe/H] agree with those derived by Mucciarelli et al. (2017) from higher resolution spectra.

4.2 AAOmega spectra

The metallicity of the stars observed with AAOmega was estimated from the strengths of their calcium triplet (CaT) lines. These lines have been used extensively in globular cluster studies to estimate the metallicity of member stars and there are a number of available empirical relationships that relate the metallicity of a star to its CaT line strengths and luminosity. In this work, as in Simpson et al. (2017), we have used Carrera et al. (2013). This calibration has a valid metallicity range of $-4.0 < $ [Fe/H] $ < +0.5$.

There are two key parameters for the CaT method: (1) the equivalent width measurements of the CaT lines (described in Section 3) and (2) the luminosity of the star. As in Simpson et al. (2017), we used the Carrera et al. (2013) empirical relationships with the absolute K_S magnitude of the star. The absolute magnitude was found using the apparent magnitudes of the stars from the 2MASS catalogue and a distance modulus of $(m - M)_{K_S} = 13.45 \pm 0.10$ (see Table 1 and Section 6 for the determination of this distance modulus.).

5 CLUSTER MEMBERSHIP

In Fig. 4, the metallicity distributions of the two samples are plotted. There is good agreement between the metallicities found from the high- and low-resolution spectra. There is a larger spread of metallicities for stars observed with AAOmega than found for HERMES, so a metallicity cut was applied to the AAOmega results that is defined as the 3σ range of the HERMES metallicity results (the vertical lines in the top panel of Fig. 4).

From the CaT method, for the 11 stars photometrically identified as clump members, and observed with AAOmega, we derive an overall metallicity of [Fe/H] $= -0.14 \pm 0.06$; for the 14 RGB members [Fe/H] $= -0.30 \pm 0.13$ and for the six SGB members [Fe/H] $= -0.09 \pm 0.13$. Overall, the metallicity estimate from the CaT method for the all 31 members observed with AAOmega was [Fe/H] $= -0.20 \pm 0.15$. As in Simpson et al. (2017), the CaT method is found to slightly underestimate the metallicity with respect to values derived from classical methods.

Most of the stars observed were farther than 10 arcmin from the cluster, with the aim of identifying 'extratidal' stars with radial velocities and metallicities matching those of cluster. From Fig. 3(b), it is clear that the stars outside the tidal radius have a wide range of radial velocities, as would be expected for a random line of sight through the Galaxy (e.g. see the results from RAVE survey; Kunder
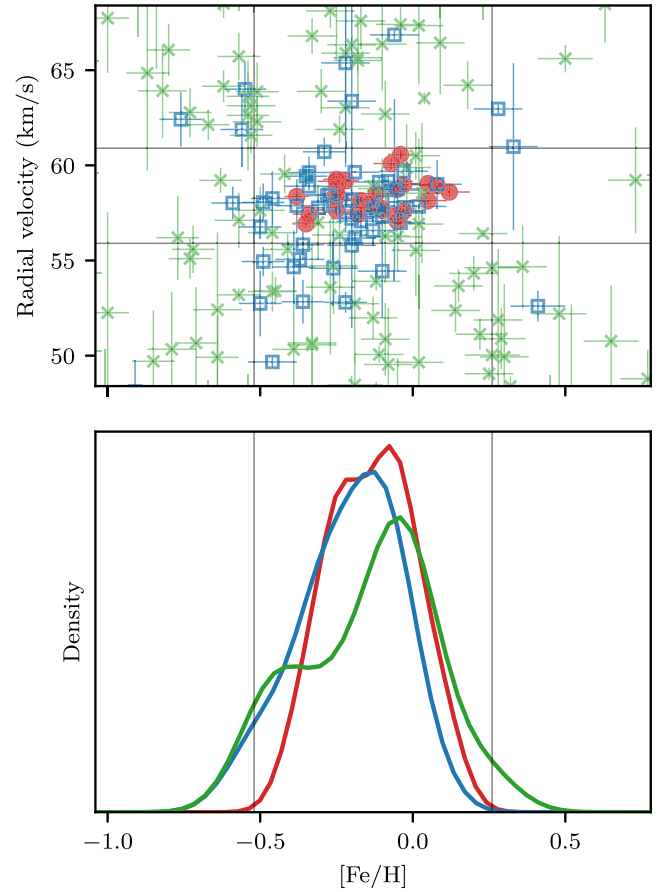

Figure 4. Top: the barycentric radial velocity of the stars against their metallicity. Red dots are stars observed with HERMES, blue squares are stars observed by AAOmega and within 10 arcmin of the cluster, and green crosses are stars observed by AAOmega and outside of 10 arcmin. The horizontal and vertical lines define the box for the membership selection. Bottom: univariate kernel density estimate (with the same bandwidth of 0.5) of the metallicity of the different samples of members.

et al. 2017). In the brighter HERMES sample, all of these stars that were within the radial velocity limits for the cluster (defined in Section 3) had bluer colours than the identified cluster members. Their positions on the CMD are not consistent with the cluster but with the field population of dwarf stars.

In the AAOmega sample, it is not as easy to exclude these large angular distance stars simply by considering their position on the CMD. The SGB and lower RGB of the cluster have the same brightness and colours as most of the field stars along the line of sight. These 'extratidal' stars were also selected with colour and magnitude cuts designed to pick out stars on the expected RGB and SGB. In the top panel of Fig. 4, we plot the distribution of the metallicity versus the radial velocity of the stars within 10 arcmin and those stars observed by AAOmega that were further out (green crosses). Using the radial velocity and metallicity limits defined by the cluster sample, there are 15 potential 'extratidal' stars of Gaia 1. Further observations of these stars will be required to determine if they are truly escaped members of the cluster.

The locations on the sky of the cluster members and field stars identified within 10 arcmin of the cluster centre are shown in Fig. 5. The radial extent of the cluster in the east–west direction on the sky is currently unclear. In the radial direction away from Sirius, it appears the edge of the cluster has been reached, as we do not find
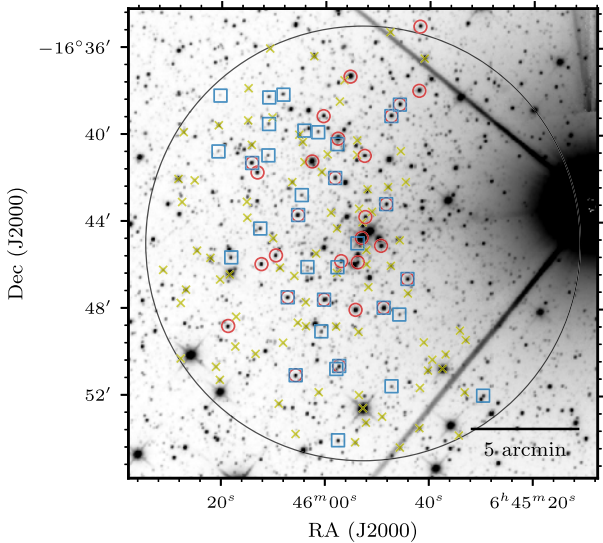
Figure 5. Sky distribution of the identified members (red circles: HERMES; blue squares: AAOmega) on the un-WISE W1 image (Lang 2014; Meisner, Lang & Schlegel 2016). Indicated with yellow crosses are field stars within 10 arcmin that were also observed. The large circle shows 10 arcmin around the cluster centre. The radial extent of the cluster is not clear as the exclusion zone around Sirius in our observing strategy (and also in 2MASS) has limited our ability to identify how far east the cluster extends on the sky.

any radial velocity members further east than RA = $6^h46^m20^s$. In the radial direction towards Sirius, the edge is our observing exclusion zone around Sirius (see Section 2). This has placed an artificial limit on the identification of members radially towards Sirius.

6 DISCUSSION

In Fig. 6, we replot the CMDs from Fig. 1, with only the identified members and potential extratidal stars. The PARSEC isochrones (version 1.2S; Bressan et al. 2012; Chen et al. 2014, 2015; Tang et al. 2014) used have been primarily fitted by eye to the brightness and colour of the red clump stars. The luminosity of the red clump has only a weak dependence on the age (e.g. Girardi 2016) and so it was used to determine the distance modulus and reddening of the clusters (Table 1). The red clump brightness, the slope of the giant branch and the turn-off magnitude are consistent with a [M/H] = −0.2 cluster with an age of about 3 Gyr.

With the aid of the spectroscopic results, we have fitted a more metal rich and younger isochrone than Koposov et al. (2017), who used a representative [Fe/H] = −0.7, 6 Gyr isochrone. This has the result of making the tip of the giant branch fainter than their prediction, and as a consequence it seems very unlikely that there are any naked eye members of Gaia 1 as suggested in the discovery paper. It is clear, however, that overall Gaia 1 is bright enough that it would have been identified earlier either with the aided eye by astronomers in the 19th or 20th century or during imaging surveys were it not hidden by the glare of Sirius.

There is a small discrepancy in the de-reddened distance moduli found using the optical and infrared photometry (Table 1). This is likely related to the transformations (from Schlafly & Finkbeiner 2011) between the different photometric systems. For two reasons the distance modulus derived from the infrared photometry is preferred: (1) there is relatively high reddening in the direction of the cluster and (2) the K_S band has been shown to

minimize the intrinsic differences in red clump star luminosities associated with metallicity (Girardi 2016).

Using this distance modulus, the cluster is found at a heliocentric distance of 4.46 ± 0.21 kpc and a Galactocentric distance of 11.5 ± 0.2 kpc ([X, Y, Z] = [11.0 ± 0.1, −3.2 ± 0.2, −0.64 ± 0.03] kpc in a left-handed coordinate frame). The cluster half-light radius 6.5 ± 0.4 arcmin (Koposov et al. 2017) translates to a physical half-light radius of 8.4 ± 0.6 pc. These coordinate transformations were performed using astropy, assuming that the cluster position has an uncertainty of 1 arcmin and astropy's default parameters that the Sun is 8.3 kpc from the Galactic Centre and 27 pc above the plane (Chen et al. 2001; Reid & Brunthaler 2004; Gillessen et al. 2009).

Schlafly & Finkbeiner (2011) and Green et al. (2015) estimated reddening values of $E(B - V) = 0.4911 \pm 0.0079$ and $E(B - V) = 0.36 \pm 0.031$, respectively, for the direction and distance of Gaia 1. Transforming the reddening value found from the isochrone fit via relationships derived from Schlafly & Finkbeiner (2011), finds,

$$E(B - V) = 2.4 \times E(J - K_S) = 0.66. \tag{1}$$

This reddening is twice what is predicted. This could be the result of the angular proximity to Sirius impacting the reddening estimates, or the accuracy of the photometry.

The metallicity we have found for Gaia 1 is higher than the mean value for open clusters at its Galactocentric distance of 11.8 kpc (e.g. Jacobson, Friel & Pilachowski 2009; Yong, Carney & Friel 2012), but it is within the distribution. The Galactic radial metallicity gradient as measured from open clusters has a transition at around $R_{GC} = 13$ kpc (e.g. Twarog, Ashman & Anthony-Twarog 1997), becoming distinctly shallower in the outer disc. The similarity in the radial metallicity gradients for open clusters of different ages is commonly interpreted to mean that the Galactic metallicity gradient has been fairly stable over time (Friel & Janes 1993), though possibly the transition radius has shifted outwards (Jacobson, Pilachowski & Friel 2011). From its position and metallicity, Gaia 1 would appear to belong to the inner disc population. However, our calculation of its orbit (Section 6.1) would appear to contradict this explanation.

Assuming that Gaia 1 is an isolated system for which the virial theorem holds, then the dynamical mass can be given by

$$M_{dyn} \simeq 2.5 \frac{3\sigma_0^2 r_h}{G} = 12.9^{+4.6}_{-3.8} \times 10^3 \, M_\odot. \tag{2}$$

This value is very close to the 14 000 $M_\odot$ estimated by Koposov et al. (2017) using the stellar density profile. The dynamical masses are dependent on the square of the velocity dispersion, and if the velocity dispersion is reduced from $\sigma_v = 0.94 \pm 0.15$ (the overall value) to 0.86 ± 0.09 km s^{-1} (derived from just the HERMES sample), this reduces the cluster mass estimate by over 1000 solar masses.

6.1 Orbit

The positional information was combined with kinematic information to estimate a probable orbit for the cluster. None of the stars identified as members were bright enough to be part of the Tycho-Gaia Astrometric Solution (TGAS; Michalik, Lindegren & Hobbs 2015; Lindegren et al. 2016), but 42 member stars were in the UCAC5 proper motion catalogue (Zacharias et al. 2017) and are shown on Fig. 7. A UCAC magnitude cut of $u_{mag} < 15$ was selected based on fig. 9 of Zacharias et al. (2017), which shows the proper
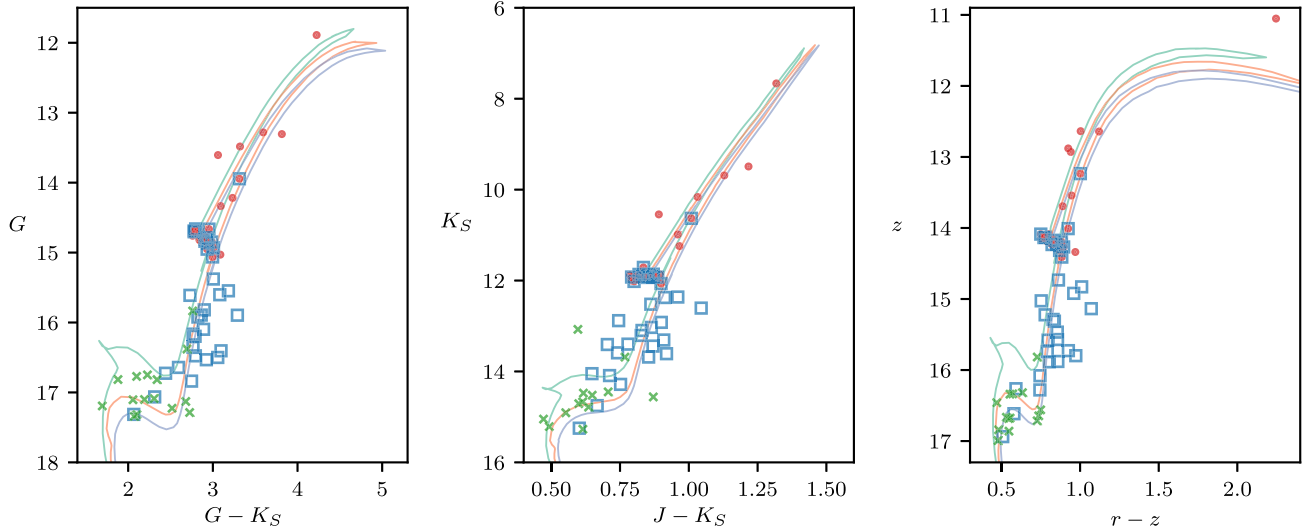
Figure 6. The CMDs in *Gaia*, 2MASS and PS1 photometry (as in Fig. 1, but showing only the probable members identified from their radial velocity and metallicity (red dots: observed with HERMES; blue squares: observed with AAOmega and $r < 10$ arcmin; green cross: observed with AAOmega and $r > 10$ arcmin). The isochrones are all for [M/H] $= -0.2$ and with ages of 2.5, 3.5, 4.5 Gyr (turn-off magnitude increases with age).
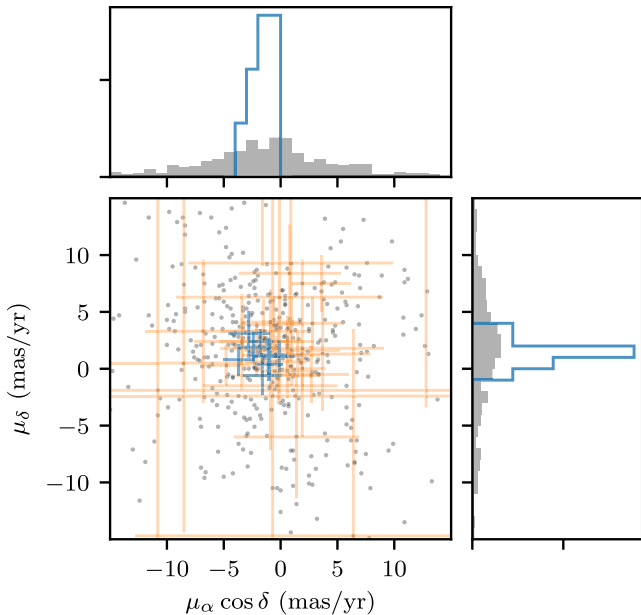

Figure 7. The UCAC5 proper motions of member stars with UCAC magnitudes less than 15 (blue error bars) and the rest of the identified members (orange crosses). The black dots are all UCAC5 targets within 12 arcmin of the cluster. The histograms show the distribution of the bright members (open blue) and all targets (shaded black histogram). A magnitude cut of 15 was selected based on fig. 9 of Zacharias, Finch & Frouard (2017), which shows the proper motion errors rapidly increasing at that brightness.

motion errors rapidly increasing at that brightness. There were nine stars that made this magnitude cut, all of which had small uncertainties in their proper motion: $\sigma(\mu_\alpha\cos\delta, \mu_\delta) < (1.8, 2.0)$ mas yr^{-1}. Their mean proper motions were $(\mu_\alpha\cos\delta, \mu_\delta) = (-1.7 \pm 0.5, 1.3 \pm 0.5)$ mas yr^{-1}.

We computed the orbits of the cluster using the GALPY code (http://github.com/jobovy/galpy; Bovy 2015, version 1.2) with inputs of $(\alpha, \delta, r_\odot, \mu_\alpha\cos\delta, \mu_\delta, v_r)$ and the recommended simple Milky Way-like MWPotential2014 potential with the default

parameters, and the Solar motion defined by Schönrich, Binney & Dehnen (2010). The cluster orbit was integrated forward in time for 1 Gyr with 1 Myr resolution, for 10 000 random realizations varying the inputs with Gaussian errors. In Fig. 8, for clarity, a subset of 100 of these realizations are shown.

The median value of the orbital parameters was found for the 10 000 realizations, with uncertainty ranges given by the 16th and 84th percentile values: the maximum and minimum Galactic distance achieved by the cluster are $r_{max} = 13.8^{+1.4}_{-1.1}$ kpc and $r_{min} = 11.4^{+0.2}_{-0.2}$ kpc; the largest distance out of the Galactic plane, $z_{max} = 1.1^{+0.4}_{-0.3}$ kpc; and the eccentricity of the orbit $e = 0.09^{+0.04}_{-0.03}$. The uncertainties in these orbital parameters are primarily driven by the uncertainty in the proper motions, with a much smaller contribution from the uncertainty in the distance. There was a negligible contribution from the uncertainty in the radial velocity and position of the cluster. The *Gaia* DR2+ results should improve the precision to which the cluster's orbit can be calculated by providing accurate and precise proper motions.

The present day finds Gaia 1 at about two-thirds of its maximum distance out of the Galactic plane. Vande Putte et al. (2010) investigated the orbits of Galactic open clusters and found that most clusters are in quasi-periodic crown orbits like that of Gaia 1. They further classified clusters based upon their z_{max} and radial quantity, defined as

$$\eta = \frac{R_{max} - R_{min}}{0.5(R_{max} + R_{min})}, \tag{3}$$

where R is the Galactocentric distance of the cluster projected on to the Galactic plane. For Gaia 1 the radial quantity is $\eta = 0.19^{+0.09}_{-0.06}$. It would be expected that clusters that formed in the disc of the Galaxy would have low η, and Vande Putte et al. (2010) found 80 per cent of the 439 clusters had $\eta < 0.28$ and 90 percent of clusters had $z_{max} < 0.35$ kpc. Although Gaia 1 has a circular orbit like the majority of open clusters, it has a large maximum distance out of the Galactic plane; over three times the scaleheight of the thin disc.

Numerical simulations of open cluster orbital evolution have shown that it is possible for the spiral arms of the Galaxy to have a large vertical effect on clusters, giving them large out-of-plane excursions (>200 pc), though these orbits tend to be chaotic
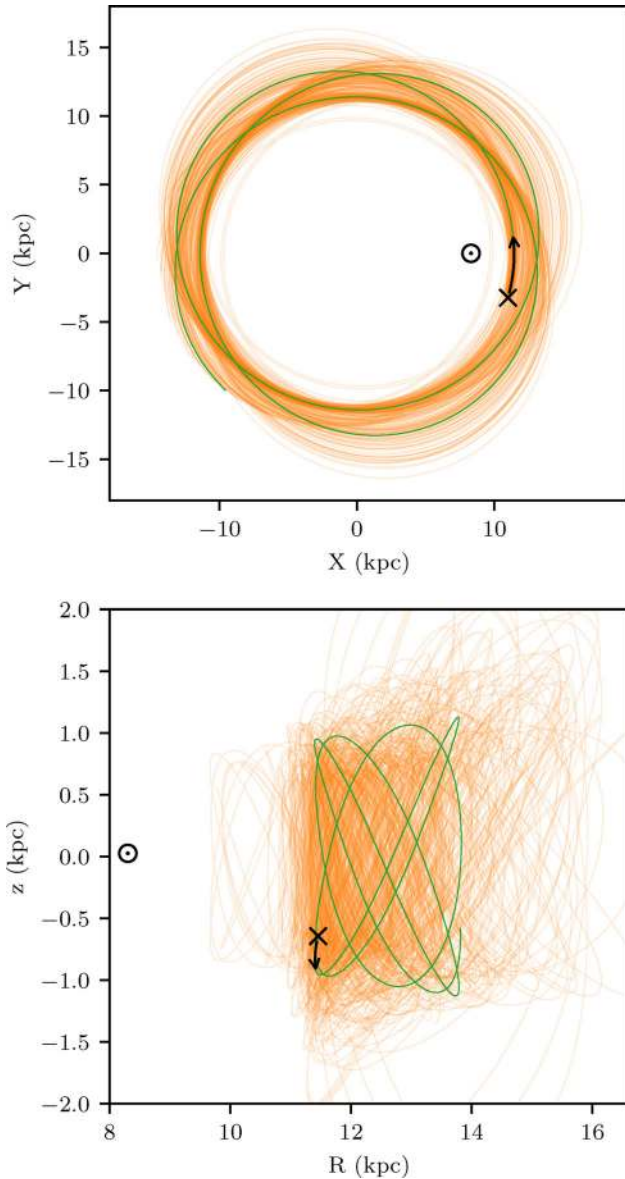
Figure 8. Projection of the orbit of Gaia 1 integrated forward in time using GALPY. The green line shows the orbit using the best values found for the cluster and the fainter orange lines show the orbits of the random realizations. The black arrow indicates the direction of motion for this 'best' orbit from the starting position. The currently observed position of Gaia 1 is marked with a cross and also shown is the present day of the Sun (☉). For clarity, only 100 of the 10 000 random realizations are shown.

(see e.g. Martinez-Medina et al. 2016). Martinez-Medina et al. (2017) investigated the survival of such high-altitude open clusters, and find that clusters in the plane of the disc and clusters with relatively large vertical motions ($z_{max} \gtrsim 3.5$ kpc) tend to have the longest lifetimes. This is because the clusters experience the tidal stresses associated with disc crossings never (in the case of clusters in the plane) or rarely (in the case of high-altitude clusters). The clusters with the shortest lifetimes (with respect to an identical cluster on an in-plane orbit) have $z_{max} \sim 600$ pc. Gaia 1, with $z_{max} \approx 1.1$ kpc, is in a region of orbital parameter space which should be quite detrimental to its long-term survival. In its present orbit, it makes nine plane crossings every gigayear, for a total of over 30 in its 3 Gyr lifetime.

It is therefore surprising to find Gaia 1 in its present orbit at the present day. This suggests that either it has recently moved into this orbit, perhaps after an interaction with a spiral arm (Martinez-Medina et al. 2016), or that it has experienced significant mass loss in the past, and is now on the verge of complete destruction. Significant mass loss in the past would tend to support the association of the extratidal stars we find with radial velocities, metallicities and photometry consistent with Gaia 1. Higher precision radial velocity measurements could help to clarify whether Gaia 1 is in virial equilibrium or whether it is in the process of disrupting.

We have presented the first spectroscopic observations of stellar cluster Gaia 1, which was recently discovered by Koposov et al. (2017). Although initially these observations were carried out to investigate the novelty of a cluster that had previously been blocked from our view by glare from Sirius, these observations have shown Gaia 1 is an interesting target in its own right, being relatively metal-rich and intermediate age cluster, and with a mass of $12.9^{+4.6}_{-3.8} \times 10^3$ M$_\odot$.

Both low- and high-resolution spectra are consistent with the cluster having a metallicity of [Fe/H] $= -0.13 \pm 0.13$. Isochrone fits indicate that the cluster is about 3 Gyr in age. Orbital modelling shows that Gaia 1 has a circular orbit but a large motion out of the plane of the Galaxy, and is currently found 640 ± 30 pc below the plane of the Galaxy and could travel as much as $z_{max} = 1.1^{+0.4}_{-0.3}$ kpc. Such an orbit could result in the cluster experiencing over 30 plane passages during its lifetime, which means that Gaia 1 could have a large stellar stream associated with it that is waiting to be discovered.

REFERENCES

AAO Software Team 2015, Astrophysics Source Code Library, record ascl:1505.015

Andrews J. J., Chanamé J., Agüeros M. A., 2017, MNRAS, preprint (arXiv:1704.07829)

Blanco-Cuaresma S., Soubiran C., Heiter U., Jofré P., 2014, A&A, 569, A111

Bovy J., 2015, ApJs, 216, 29

Bressan A., Marigo P., Girardi L., Salasnich B., Dal Cero C., Rubele S., Nanni A., 2012, MNRAS, 427, 127

Brown A. G. A. et al., 2016, A&A, 595, A2

Carrera R., Pancino E., Gallart C., del Pino A., 2013, MNRAS, 434, 1681

Castelli F., Kurucz R. L., 2004, preprint (arXiv:0405087)

Chambers K. C. et al., 2016, preprint (arXiv:1612.05560)

Chen B. et al., 2001, ApJ, 553, 184

Chen Y., Girardi L., Bressan A., Marigo P., Barbieri M., Kong X., 2014, MNRAS, 444, 2525

Chen Y., Bressan A., Girardi L., Marigo P., Kong X., Lanza A., 2015, MNRAS, 452, 1068

De Silva G. M. et al., 2015, MNRAS, 449, 2604

Edlén B., Risberg P., 1956, Ark. Fys., 10, 553

Friel E. D., Janes K. A., 1993, A&A, 267, 75

Gillessen S., Eisenhauer F., Trippe S., Alexander T., Genzel R., Martins F., Ott T., 2009, ApJ, 692, 1075

Girardi L., 2016, ARA&A, 54, 95

Green G. M. et al., 2015, ApJ, 810, 25

Han E., Curtis J. L., Wright J. T., 2016, AJ, 152, 7

Jacobson H. R., Friel E. D., Pilachowski C. A., 2009, AJ, 137, 4753

Jacobson H. R., Pilachowski C. A., Friel E. D., 2011, AJ, 142, 59

Jordi C. et al., 2010, A&A, 523, A48

Koposov S. et al., 2007, ApJ, 669, 337

Koposov S. E., Belokurov V., Torrealba G., Evans N. W., 2015, ApJ, 805, 130

Koposov S. E., Belokurov V., Torrealba G., 2017, MNRAS, 470, 2702

Kunder A. et al., 2017, AJ, 153, 75

Lang D., 2014, AJ, 147, 108

Lewis I. J. et al., 2002, MNRAS, 333, 22

Lindegren L. et al., 2016, A&A, 595, A4

Loden L. O., 1980, A&AS, 41, 173

Magnier E. A. et al., 2016, preprint (arXiv:1612.05242)

Martell S. L. et al., 2017, MNRAS, 465, 3203

Martinez-Medina L. A., Pichardo B., Moreno E., Peimbert A., Velazquez H., 2016, ApJ, 817, L3

Martinez-Medina L. A., Pichardo B., Peimbert A., Moreno E., 2017, ApJ, 834, 58

Massari D., Posti L., Helmi A., Fiorentino G., Tolstoy E., 2017, A&A, 598, L9

McKinney W., 2010, in van der Walt S., Millman J., eds, Proc. 9th Python Sci. Conf. pp 51

McLean A., Mitchell C., Swanston D., 1994, J. Electron Spectrosc. Relat. Phenom., 69, 125

Meisner A. M., Lang D., Schlegel D. J., 2016, AJ, 153, 38

Mermilliod J.-C., Paunzen E., 2003, A&A, 410, 511

Merrifield M. R., Gray M. E., Haran B., 2016, preprint (arXiv:1612.00834)

Michalik D., Lindegren L., Hobbs D., 2015, A&A, 574, A115

Miszalski B., Shortridge K., Saunders W., Parker Q. A., Croom S. M., 2006, MNRAS, 371, 1537

Mucciarelli A., Monaco L., Bonifacio P., Saviane I., 2017, A&A, 603

Oh S., Price-Whelan A. M., Hogg D. W., Morton T. D., Spergel D. N., 2017, AJ, 153, 257

Prusti T. et al., 2016, A&A, 595, A1

Reid M. J., Brunthaler A., 2004, ApJ, 616, 872

Robitaille T., Bressert E., 2012, Astrophysics Source Code Library, record: ascl:1208.017

Robitaille T. P. et al., 2013, A&A, 558, A33

Schlafly E. F., Finkbeiner D. P., 2011, ApJ, 737, 103

Schönrich R., Binney J., Dehnen W., 2010, MNRAS, 403, 1829

Sharp R. et al., 2006, in McLean I. S., Iye M., eds, Proc. SPIE Conf. Ser. Vol. 6269, Ground-based and Airborne Instrumentation for Astronomy. SPIE, Bellingham, p. 62690G

Sheinis A. et al., 2015, J. Astron. Telescopes Instrum. Syst., 1, 035002

Simpson J. D., Silva G. D., Navin C. A., Martell S. L., Zucker D. B., 2017, preprint (arXiv:1703.03823)

Skrutskie M. F. et al., 2006, AJ, 131, 1163

Sneden C., 1973, PhD thesis, The University of Texas at Austin

Sousa S. G., Santos N. C., Adibekyan V., Delgado-Mena E., Israelian G., 2015, A&A, 577, A67

Tang J., Bressan A., Rosenfield P., Slemer A., Marigo P., Girardi L., Bianchi L., 2014, MNRAS, 445, 4287

Taylor M., 2005, in Shopbell P., Britton M., Ebert R., eds, ASP Conf. Ser. Vol. 347, Astronomical Data Analysis Software and Systems XIV. p. 29

Twarog B. A., Ashman K. M., Anthony-Twarog B. J., 1997, AJ, 114, 2556

Vande Putte D., Garnier T. P., Ferreras I., Mignani R. P., Cropper M., 2010, MNRAS, 407, 2109

Watkins L. L., van der Marel R. P., 2017, ApJ, 839, 89

Yong D., Carney B. W., Friel E. D., 2012, AJ, 144, 95

Zacharias N., Finch C., Frouard J., 2017, AJ, 153, 166

APPENDIX A: LINE LIST

Table A1. The line list used for the HERMES stellar parameter determination.

λ (Å)	Element	EP (eV)	log *gf*
4788.757	Fe I	3.237	−1.763
4794.360	Fe I	2.424	−3.950
4802.880	Fe I	3.642	−1.510
4808.148	Fe I	3.251	−2.690
4834.517	Fe I	2.420	−3.330
4890.755	Fe I	2.875	−0.394
4891.492	Fe I	2.851	−0.111
5651.469	Fe I	4.473	−1.900
5652.318	Fe I	4.260	−1.850
5661.346	Fe I	4.284	−1.756
5679.023	Fe I	4.652	−0.820
5696.090	Fe I	4.548	−1.720
5701.557	Fe I	2.560	−2.160
5704.733	Fe I	5.033	−1.409
5705.465	Fe I	4.301	−1.355
5720.898	Fe I	4.548	−1.631
5731.762	Fe I	4.256	−1.200
5732.296	Fe I	4.991	−1.460
5741.848	Fe I	4.256	−1.672
5752.032	Fe I	4.549	−1.177
5775.081	Fe I	4.220	−1.297
5778.453	Fe I	2.588	−3.430
5806.724	Fe I	4.607	−1.030
5809.218	Fe I	3.883	−1.790
5853.148	Fe I	1.485	−5.180
5855.077	Fe I	4.608	−1.478
5858.778	Fe I	4.220	−2.160
5861.110	Fe I	4.283	−2.304
5862.357	Fe I	4.549	−0.127
6494.994	Fe I	2.400	−1.256
6498.939	Fe I	0.958	−4.688
6546.239	Fe I	2.758	−1.536
6592.914	Fe I	2.727	−1.473
6593.870	Fe I	2.433	−2.420
6597.561	Fe I	4.795	−0.970
6627.545	Fe I	4.548	−1.580
6653.853	Fe I	4.154	−2.215
6677.987	Fe I	2.692	−1.418
6699.142	Fe I	4.593	−2.101
6703.567	Fe I	2.758	−3.060
6705.101	Fe I	4.607	−1.392
6710.319	Fe I	1.485	−4.764
6713.745	Fe I	4.795	−1.500
6725.357	Fe I	4.103	−2.013
6726.667	Fe I	4.607	−1.133
6733.151	Fe I	4.638	−1.480
7710.364	Fe I	4.220	−1.113
7723.210	Fe I	2.280	−3.617
7748.269	Fe I	2.949	−1.751
7751.109	Fe I	4.991	−0.783
7780.556	Fe I	4.473	−0.010
7802.473	Fe I	5.086	−1.417
7807.909	Fe I	4.991	−0.521
7844.559	Fe I	4.835	−1.759
4720.150	Fe II	3.197	−4.822
4731.453	Fe II	2.891	−3.127
4833.197	Fe II	2.657	−4.795
6516.080	Fe II	2.891	−3.432
7711.723	Fe II	3.903	−2.683
7841.390	Fe II	3.900	−3.896

APPENDIX B: CLUSTER MEMBERS

Table B1. Parameters for members of Gaia 1 observed with HERMES.

Gaia source_id	PS1 objID	r (arcmin)	SNR1	SNR2	SNR3	SNR4	v_r (km s^{-1})	T_{eff} (K)	log g_{spec}	log g_{phot}	[Fe/H]
2946299839381625344	87771015236028832	7.70	10	19	32	32	57.4 ± 0.3	5200	3.5	2.7	− 0.18 ± 0.05
2946300011181433856	87781014887617472	6.86	8	15	25	25	60.1 ± 0.6	5400	4.0	2.8	− 0.07 ± 0.06
2946300423497294336	87821015778053968	7.53	10	19	30	30	57.4 ± 0.4	5400	3.5	2.7	− 0.05 ± 0.05
2946300664016492032	87851015301440560	4.68	11	20	33	32	57.0 ± 0.3	5300	3.6	2.7	− 0.05 ± 0.05
2946301041973608960	87831014757969200	4.26	15	31	58	57	60.6 ± 0.4	4900	3.1	2.1	− 0.04 ± 0.04
2946301076335192064	87841015010738448	3.98	9	17	29	26	58.6 ± 0.6	5600	4.3	2.9	0.12 ± 0.07
2946301145053017600	87841014533031232	4.43	14	28	49	50	58.0 ± 0.5	4700	2.5	2.1	− 0.14 ± 0.04
2946301557369703424	87881015512560992	4.63	11	20	44	31	58.1 ± 0.3	5400	3.7	2.8	− 0.17 ± 0.06
2946301557369708544	87881015396809088	3.86	10	17	31	31	58.9 ± 0.4	5150	3.1	2.7	0.08 ± 0.05
2946301729168396800	87881014741582944	2.10	13	22	33	35	57.7 ± 0.6	5450	3.6	2.7	− 0.10 ± 0.04
2946301729168397824	87881014874583952	2.07	8	14	29	28	57.6 ± 0.6	5300	3.5	2.7	− 0.25 ± 0.07
2946303378435861504	87921015220436288	2.42	9	18	29	31	58.2 ± 0.4	–	–	–	–
2946303550234568704	87961015546585312	4.75	8	15	25	26	57.4 ± 0.4	5300	3.5	2.8	− 0.34 ± 0.05
2946303550234570752	87971015589864016	5.17	8	15	29	28	59.3 ± 0.5	5250	3.5	2.7	− 0.25 ± 0.04
2947051836616382464	87861014343327792	3.86	10	17	29	28	57.6 ± 0.3	5400	4.7	2.8	− 0.03 ± 0.06
2947052042774817792	87891014555928208	1.92	16	29	57	49	58.3 ± 0.4	4950	2.9	2.3	− 0.25 ± 0.04
2947052352012464128	87901014709095408	1.08	21	54	-89	137	59.3 ± 0.5	–	–	–	–
2947052455091682304	87921014682294608	0.68	15	24	36	36	57.6 ± 0.5	5300	3.0	2.7	− 0.10 ± 0.05
2947052729969764864	87931014515586560	1.74	8	14	29	27	58.7 ± 0.6	5400	3.7	2.8	− 0.05 ± 0.05
2947054276155475968	87961014925020480	1.94	14	24	34	36	58.8 ± 0.4	5100	2.5	2.6	− 0.25 ± 0.05
2947054310515227648	87971015108695600	3.12	14	34	540	73	56.9 ± 0.5	4900	2.8	2.0	− 0.35 ± 0.05
2947054379234722304	87991014902006688	3.66	16	35	88	72	58.4 ± 0.8	4450	2.2	1.7	− 0.38 ± 0.04
2947055100791549952	87981014689160944	2.90	12	19	38	34	59.2 ± 0.6	5400	3.2	2.7	− 0.25 ± 0.06
2947055272587941888	88011015019007344	4.82	10	17	32	31	59.2 ± 0.7	5100	3.0	2.6	− 0.22 ± 0.04
2947055375669662720	88011014476597600	5.02	13	21	35	35	59.0 ± 0.6	5200	2.7	2.6	0.05 ± 0.06
2947055444388945408	88021014409238176	5.66	9	16	35	31	58.1 ± 0.9	6000	4.4	2.9	0.05 ± 0.06
2947055547465894400	88051014804973792	6.47	16	33	67	63	58.5 ± 0.6	4500	2.5	1.8	− 0.25 ± 0.04
2947058399326636032	88041014253730976	6.62	14	25	46	43	59.0 ± 0.6	4950	3.5	2.4	− 0.03 ± 0.07
2947058914722539520	88101014246980016	9.34	13	22	39	38	58.5 ± 0.5	5200	3.2	2.6	− 0.12 ± 0.07

Table B2. Parameters for members of Gaia 1 observed with AAOmega.

Gaia source_id	PS1 objID	r (arcmin)	SNR	v_r (km s^{-1})	[Fe/H]
2946293723347668992	87711014894919104	9.13	71	58.0 ± 1.7	-0.49 ± 0.07
2946294719781718016	87761013733870656	8.92	58	58.9 ± 0.3	-0.34 ± 0.08
2946294822860913664	87761014467728992	6.70	32	57.9 ± 0.1	-0.26 ± 0.07
2946299839381625344	87771015236028832	6.81	52	57.1 ± 1.3	-0.17 ± 0.08
2946300011181433856	87781014910484720	5.91	36	59.6 ± 1.5	-0.34 ± 0.07
2946300011181433856	87781014887617472	5.75	52	59.1 ± 0.5	-0.11 ± 0.08
2946300217339877888	87811015031489296	4.48	51	59.4 ± 0.9	-0.35 ± 0.07
2946300664016492032	87851015301440560	4.26	49	57.6 ± 0.6	-0.12 ± 0.08
2946301076335192064	87841015010738448	3.15	46	58.4 ± 0.3	-0.28 ± 0.08
2946301145053017600	87841014533031232	3.11	65	58.1 ± 1.3	-0.10 ± 0.10
2946301179412755456	87831014407495008	3.67	47	58.3 ± 2.5	-0.46 ± 0.07
2946301488650226176	87871015144668416	2.78	32	60.7 ± 1.3	-0.29 ± 0.07
2946301660448917504	87871014904248352	1.61	26	58.8 ± 1.2	-0.05 ± 0.08
2946303103557947392	87911015523073776	4.78	31	58.5 ± 1.2	-0.27 ± 0.08
2946303550234570752	87971015589864016	6.30	40	59.7 ± 0.5	-0.03 ± 0.08
2946303893831958016	87981015859664576	7.88	21	59.0 ± 2.2	0.08 ± 0.08
2947051836616382464	87861014343327792	2.62	52	56.6 ± 1.4	-0.13 ± 0.08
2947052352012463104	87901014745180368	0.26	34	56.2 ± 0.5	-0.19 ± 0.07
2947052729969764864	87931014515586560	2.10	48	58.2 ± 1.0	-0.20 ± 0.08
2947054001280092672	87941015191724624	3.59	34	57.9 ± 2.4	-0.38 ± 0.07
2947054173076278784	87981015460201088	5.95	33	56.8 ± 1.1	-0.50 ± 0.07
2947054276155475968	87961014925020480	3.27	42	59.6 ± 0.1	-0.19 ± 0.08
2947054379234717184	87991014908411616	4.72	27	57.0 ± 1.4	-0.04 ± 0.08
2947054452254690304	88001015172583952	5.85	25	58.7 ± 8.3	-0.06 ± 0.08
2947054482313943040	88001015061852496	5.51	26	57.2 ± 0.9	-0.20 ± 0.07
2947054619752901632	88001015455799920	6.99	20	57.5 ± 1.9	-0.22 ± 0.07
2947054791551624704	88031015844675936	9.45	17	57.8 ± 0.2	0.02 ± 0.09
2947054860271100928	88031015454464384	7.98	30	57.3 ± 0.7	-0.10 ± 0.08
2947054928990581760	88031015341416976	7.76	53	57.8 ± 1.2	-0.31 ± 0.07
2947055375669662720	88011014476597600	6.00	45	59.2 ± 0.5	-0.08 ± 0.08
2947055444388945408	88021014409238176	6.61	49	57.8 ± 1.3	-0.13 ± 0.08

This paper has been typeset from a TEX/LATEX file prepared by the author.